Chemical Science

ROYAL SOCIETY OF CHEMISTRY

EDGE ARTICLE

View Article Online
View Journal | View Issue

Cite this: *Chem. Sci.*, 2025, **16**, 22638

All publication charges for this article have been paid for by the Royal Society of Chemistry

Precision pore engineering *via* fit-topology assembly in a Zn-porphyrin MOF for selective C_2H_2 capture

Zhenliang Zhu,[a] Jianfei Xiao,[a] Min Zhang,[a] Yaoqi Huang*[ab] and Shaojun Yuan *[a]

The topology-guided design of porphyrin-based metal–organic frameworks (PMOFs) with tailored ultramicroporosity (<7 Å) remains a formidable challenge, as conventional strategies often fail to balance structural rigidity with precise pore confinement. To address this limitation, we propose a dual-ligand coordination approach, integrating Zn^{2+}-porphyrin chelation and triazole-mediated SBU assembly, to construct Zn-TCPP-dmtrz—a novel PMOF featuring a unique fit topology for C_2H_2/CO_2 separation. Unlike traditional PMOFs with oversized pores (*e.g.*, Al/Y-TCPP), this strategy exploits the synergistic coordination of tetrakis(4-carboxyphenyl)porphyrin (TCPP) and 3,5-dimethyl-1,2,4-triazole (dmtrz) to compress pore apertures to 6.3 × 6.8 Å, closely matching the molecular dimensions of the C_2H_2 molecule. The resulting ultramicroporous channels, reinforced by staggered porphyrin planes and hydrophobic methyl groups, exhibit high C_2H_2 uptake (4.30 mmol g^{-1}) and a separation potential (ΔQ = 1.62 mmol g^{-1}) under ambient conditions, outperforming existing PMOFs. Crucially, the framework retains structural integrity under high humidity (90% RH) and cyclic adsorption–desorption, with a low regeneration energy barrier (Q_{st} = 28.5 kJ mol^{-1}). Computational studies attribute the selectivity to confinement-enhanced van der Waals interactions and electrostatic alignment at the porphyrin-Zn interface and methyl-decorated channels. This work establishes a topology-driven pore engineering strategy for PMOFs, advancing the design of next-generation adsorbents for challenging gas separations.

Received 22nd September 2025
Accepted 21st October 2025

DOI: 10.1039/d5sc07319g

rsc.li/chemical-science

1. Introduction

Metal–organic frameworks (MOFs) are a versatile class of crystalline porous materials assembled from metal ions or clusters and multitopic organic ligands into periodic architectures.[1–3] Their modularity not only affords ultrahigh surface areas and permanent porosity but also enables precise control over pore structures and functionalities.[4–6] These attributes have made MOFs attractive candidates for applications in gas storage and separation,[7–9] heterogeneous catalysis,[10,11] and chemical sensing.[12] One of the fundamental challenges in this field is the translation of structural diversity into rationally designed pore systems capable of delivering predictable adsorption properties and effective separation of small molecules with closely similar physicochemical characteristics.

The network topology of a MOF provides a critical link between local coordination environments and global material properties.[13,14] While metal–ligand coordination defines primary connectivity, the resulting topology dictates the dimensionality of channels, the continuity of pore windows, and the overall packing density of the framework.[15] These features directly impact how guest molecules are confined and interact within the pore space.[16–18] Even subtle variations in connectivity or linker orientation can reshape pore apertures, reorganize channels, and ultimately transform adsorption behavior.[19,20] Accordingly, rational topology engineering, guided by reticular chemistry principles, has become an effective strategy for constructing MOFs with precisely tuned pore systems.[21]

Such considerations are particularly important for the separation of small gas molecules with similar physicochemical properties. Acetylene (C_2H_2) and carbon dioxide (CO_2), for example, both have kinetic diameters of ~3.3 Å and similar polarizabilities, making size-based discrimination extremely challenging.[22,23] Their quadrupole moments, however, differ substantially (C_2H_2: -29×10^{-40} C m^2; CO_2: -14×10^{-40} C m^2), offering an opportunity for frameworks with confined pores and well-distributed adsorption sites to selectively recognize one molecule over the other.[24–26] Topology-directed pore confinement thus provides a powerful means to amplify such differences, enabling MOFs to achieve separation performance that cannot be obtained through simple surface functionalization.[27,28]

[a]*Low-carbon Technology & Chemical Reaction Engineering Lab, School of Chemical Engineering, Sichuan University, Chengdu 610065, China. E-mail: ysj@scu.edu.cn; Fax: +86-028-85405201; Tel: +86-028-85405201*

[b]*School of Engineering and Applied Sciences, Harvard University, MA 02138, USA. E-mail: yhua@seas.harvard.edu*

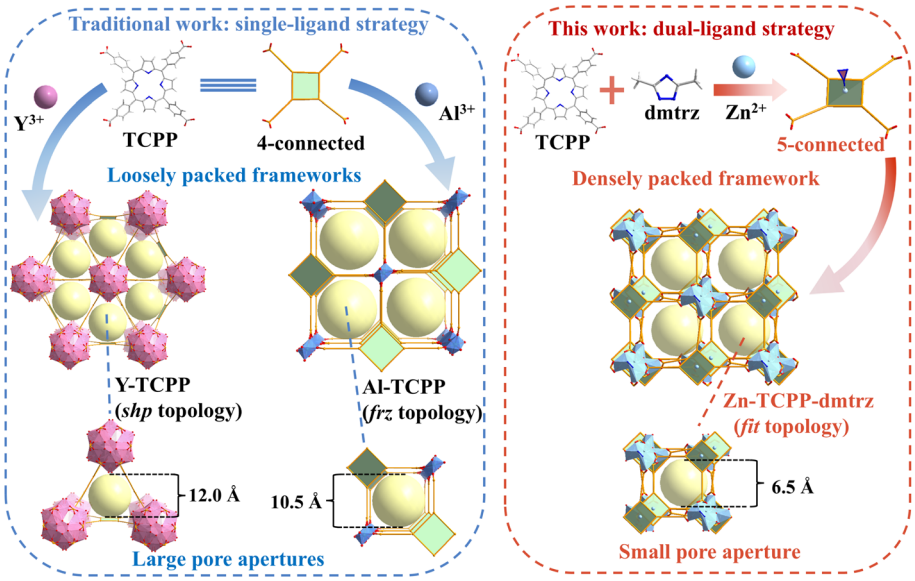

Scheme 1 Topology-directed dual-ligand strategy for pore-window compression in porphyrinic MOFs.

Porphyrin-based MOFs (PMOFs) represent a promising but underexplored platform for implementing this concept. The rigid, square-planar geometry of porphyrin ligands promotes ordered frameworks, while their π-conjugated cores impart stability and tunability.[29,30] Among them, tetrakis(4-carboxyphenyl)porphyrin (TCPP) has been most widely employed, as its four carboxylate groups readily coordinate with high-valent metals.[31,32] However, when combined with metals such as Al^{3+} or Y^{3+}, TCPP typically forms frameworks with large one-dimensional channels (>10 Å).[33,34] These structures are chemically stable but suffer from loose packing and oversized pore apertures, thereby limiting their ability to discriminate between small molecules. Attempts with transition metals such as Zn^{2+} or Cu^{2+} can, in principle, yield more compact frameworks since these metals can also coordinate to the porphyrin core.[35,36] Nevertheless, most reported transition-metal PMOFs crystallize as layered structures or interpenetrated networks, leading to limited porosity and reduced tunability.[37–39] Traditional single-ligand PMOFs (*e.g.*, Al- and Y-TCPP) therefore produce loosely packed frameworks with large pore apertures, whereas the dual-ligand approach, by introducing an auxiliary triazole ligand, converts TCPP into a 5-connected node and directs the assembly of densely packed frameworks with compressed pore windows (Scheme 1).

Building on this rationale, short N-donor linkers such as imidazoles and triazoles provide an effective means of stabilizing high-connectivity secondary building units (SBUs), suppressing interpenetration, and guiding frameworks toward compact topologies.[40–42] Integrating such linkers with porphyrins offers a powerful means to merge the rigidity of porphyrins with tunable pore confinement, yet this dual-ligand approach has rarely been applied in porphyrinic systems. In this work, we report a new PMOF, Zn-TCPP-dmtrz, synthesized from Zn^{2+}, TCPP, and 3,5-dimethyl-1,2,4-triazole (dmtrz). The introduction of dmtrz converts TCPP into a 5-connected node, which, together with Zn SBUs, directs the formation of a distinctive (5,10)-connected ***fit*** topology. The resulting framework is densely packed and features one-dimensional rectangular channels with ultramicroporous apertures of 6.3 × 6.8 Å. Compared with conventional Al- and Y-TCPP analogues, this design compresses pore size and enhances confinement, enabling more effective recognition of C_2H_2 relative to CO_2. Static adsorption isotherms at 298 K and 1 bar reveal preferential C_2H_2 uptake (4.30 mmol g^{-1}) over CO_2 (2.61 mmol g^{-1}), with a separation potential (ΔQ) of 1.6 mmol g^{-1} for equimolar C_2H_2/CO_2 mixtures—substantially higher than conventional TCPP-based MOFs. Dynamic breakthrough experiments demonstrate stable C_2H_2/CO_2 separation over 5 cycles, while static adsorption–desorption tests confirm full retention of capacity after 10 cycles, underscoring the framework's robust recyclability. Even under high humidity (90% RH), Zn-TCPP-dmtrz preserves its separation performance without noticeable degradation. The relatively low initial isosteric heat of adsorption (28.5 kJ mol^{-1} for C_2H_2) suggests facile regeneration, a critical advantage for industrial applications. Moreover, Grand Canonical Monte Carlo (GCMC) simulations and density functional theory (DFT) calculations reveal that C_2H_2 molecules preferentially adsorb at the porphyrin-Zn interface, where confinement-enhanced van der Waals interactions dominate. This work pioneers a topology-guided design strategy for PMOFs, demonstrating how coordination-driven pore compression can unlock their potential for precision gas separations.

2. Results and discussion

Zn-TCPP-dmtrz was synthesized through a solvothermal reaction of $Zn(NO_3)_2 \cdot 6H_2O$, TCPP, and dmtrz in a mixed solution of *N*,*N*-dimethylformamide (DMF), water, and a minimal amount of HNO_3 at 140 °C for 72 hours, yielding black-purple block-

shaped crystals. Single-crystal X-ray diffraction (SCXRD) studies reveal that the structure of Zn-TCPP-dmtrz belongs to the monoclinic crystal system and *C*2 space group (Table S1). Structural analysis identifies three distinct Zn^{2+} coordination environments (Fig. 1a and S1): the first Zn center adopts a five-coordinate geometry, ligated by three oxygen atoms from two carboxylate groups of adjacent TCPP ligands, one nitrogen atom from a dmtrz ligand, and one oxygen atom from a μ_3-OH group; the second Zn center exhibits a six-coordinate octahedral geometry, coordinated to four carboxylate oxygen atoms from four distinct TCPP ligands and two μ_3-OH oxygen atoms; and the third Zn center is chelated within the porphyrin macrocycle, coordinating to four nitrogen atoms of the porphyrin core and axially binding to a nitrogen atom from a dmtrz ligand, forming a five-coordinate square pyramidal geometry. This unusual axial coordination mode at the porphyrin center arises directly from the dense packing of the framework. The assembly of a pentanuclear Zn cluster—comprising four five-coordinate Zn ions and one six-coordinate Zn ion (Fig. 1a)—shortens the interlayer distance between adjacent porphyrin planes, sterically hindering ligand binding at the opposite axial site (Fig. 1b). Consequently, the porphyrin-chelated Zn center adopts an asymmetric five-coordinate geometry, bonding exclusively to a single dmtrz ligand. This multimodal coordination strategy drives the formation of two distinct secondary building units (SBUs) (Fig. 1a and b): a pentanuclear Zn cluster acting as a 10-connected node through linkages to eight TCPP carboxylates and two dmtrz ligands, and a 5-connected TCPP unit formed by the porphyrin-chelated Zn center, which bridges four carboxylate-linked Zn clusters and one axial dmtrz ligand. The interconnection of these SBUs, mediated by tritopic dmtrz spacers, generates a three-dimensional framework with a novel (5,10)-connected ***fit*** topology in porous coordination polymers (Fig. 1c), marking the first example of this topology in metal–organic frameworks. The framework features unidirectional rectangular channels along the *c*-axis (Fig. 1d and e), with pore dimensions of 6.3 × 6.8 Å, as determined by Connolly surface analysis (Fig. 1f). Notably, the staggered arrangement of porphyrin planes and Zn clusters at all four channel corners (Fig. 1e) creates a confined ultramicroporous environment, distinct from conventional PMOFs, where partial corner occupation by elongated metal-carboxylate chains or vertically aligned porphyrins leads to larger apertures. This asymmetric distribution of SBUs compresses the pore aperture into the ultramicroporous regime while introducing a diverse chemical environment: the π-conjugated porphyrin walls enhance the van der Waals interactions with C_2H_2, facilitating its selective adsorption in C_2H_2/CO_2 mixtures, while the hydrophobic methyl groups of dmtrz ligands project into the channels, minimizing competitive H_2O adsorption that could otherwise interfere with the C_2H_2 recognition.

The phase purity and structural integrity of Zn-TCPP-dmtrz are confirmed by powder X-ray diffraction (PXRD, Fig. S2). The experimental patterns of both the as-synthesized and activated samples closely match the simulated pattern derived from single-crystal data. Scanning electron microscopy (SEM) images, presented in Fig. S3a, reveal uniform block-shaped particles with sizes ranging from 50 to 100 μm. Elemental mapping *via* SEM-EDX (Fig. S3b) shows a homogeneous distribution of C, N, O, and Zn across the framework, which is further

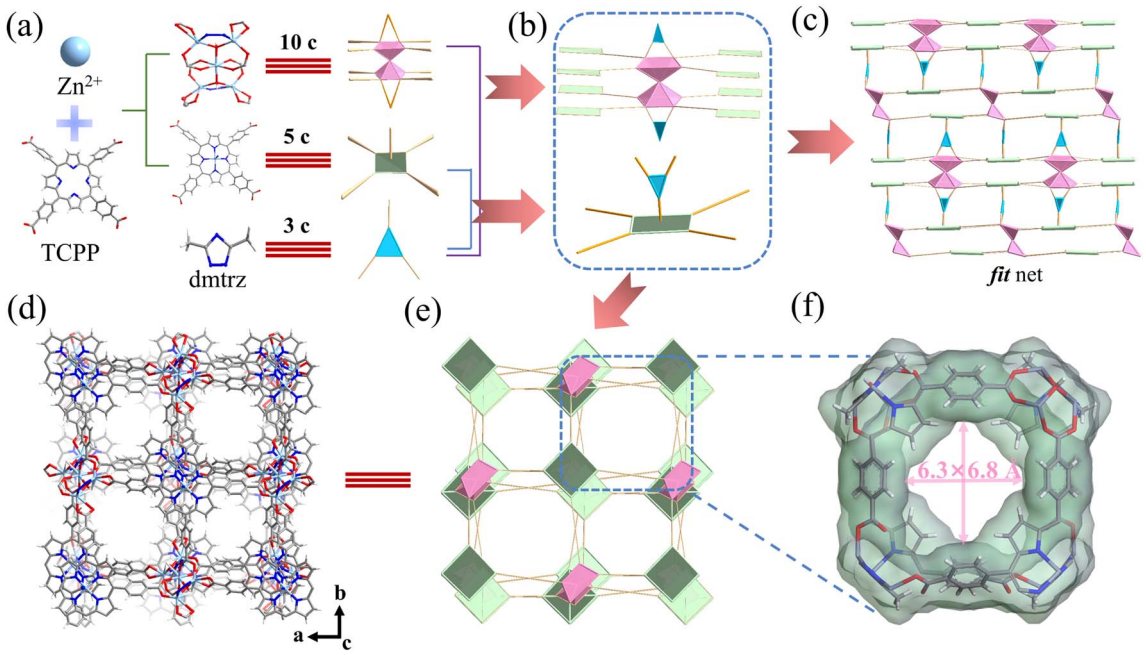

Fig. 1 (a) The structure of the building blocks of Zn-TCPP-dmtrz and the corresponding polyhedral model; (b) polyhedral simplification of the SBUs; (c) the (5,10)-connected ***fit*** topology of Zn-TCPP-dmtrz; (d) 3D framework of Zn-TCPP-dmtrz along the *c*-axis; (e) polyhedral view of the framework structure; (f) Connolly surface representation of the pores in Zn-TCPP-dmtrz. Color code: Zn, light blue; O, red; N, blue; C, gray; H, white.

confirmed by X-ray photoelectron spectroscopy (XPS) data (Fig. S4). According to the single-crystal X-ray diffraction results (CCDC 2410049) and the XPS elemental composition, the molecular formula of Zn-TCPP-dmtrz is determined to be $Zn_7(\mu_3\text{-}OH)_2(TCPP)_2(dmtrz)_2(DMF)_2$. The XPS analysis confirms the presence of Zn^{2+}, with a binding energy of 1021.9 eV for the Zn $2p_{3/2}$ peak, and provides information about the coordination environment of nitrogen species, including triazole N at 399.8 eV and pyrrolic N at 401.7 eV (Fig. S5).[43] Fourier-transform infrared spectroscopy (FT-IR, Fig. S6) reveals characteristic peaks at 1119.5 and 1347.0 cm^{-1} corresponding to C–N stretching vibrations of the porphyrin ring, at 989.2 cm^{-1} for N–N stretching in dmtrz ligands, and at 531.4 and 429.7 cm^{-1} for Zn–O and Zn–N bonds, respectively.[44] The N_2 adsorption isotherm at 77 K (Fig. S7) exhibits a type I adsorption curve, characteristic of microporous materials, with a calculated Brunauer–Emmett–Teller (BET) surface area of 829 $m^2\ g^{-1}$ and a pore volume of 0.34 $cm^3\ g^{-1}$. Non-local density functional theory (NLDFT) calculations show a narrow pore size distribution centered at 0.5–0.8 nm, which aligns well with the crystallographic pore dimensions. Thermogravimetric analysis (TGA, Fig. S8) shows that the framework remains stable up to 380 °C before decomposition begins, demonstrating its excellent thermal stability. Overall, these comprehensive characterization studies confirm the successful synthesis of Zn-TCPP-dmtrz as a highly crystalline, thermally stable, and ultramicroporous material, making it suitable for gas separation applications.

Inspired by its ultramicroporous characteristics, the adsorption performance and separation potential of Zn-TCPP-dmtrz for C_2H_2 and CO_2 are systematically examined. As shown in Fig. 2a, single-component adsorption isotherms for both gases are measured at various temperatures using a BSD-660M sorption analyzer (BSD Instruments). The results clearly indicate a stronger affinity for C_2H_2 than for CO_2 under identical conditions. Specifically, at 298 K and 1 bar, Zn-TCPP-dmtrz exhibits a C_2H_2 adsorption capacity of 4.30 mmol g^{-1}, outperforming several well-established porous materials, such as SOFOUR-TEPE-Zn (3.98 mmol g^{-1}),[45] ZJU-74 (3.83 mmol g^{-1}),[46] JNU-1 (3.35 mmol g^{-1}),[47] Zn-bpy-DLmal (3.10 mmol g^{-1}),[48] and NKMOF-1-Ni (2.74 mmol g^{-1})[49] (Table S4). In contrast, the CO_2 uptake is considerably lower, with Zn-TCPP-dmtrz adsorbing only 2.61 mmol g^{-1} under the same conditions. Furthermore, when the temperature is adjusted to 283 K or 313 K, the C_2H_2 uptake remains significantly higher than that of CO_2 at both temperatures, reaffirming the stronger interaction between C_2H_2 and the framework. To better understand the differences in C_2H_2 and CO_2 adsorption behavior across TCPP-based adsorbents, we synthesize seven different TCPP-based PMOFs incorporating various metals, comparing their C_2H_2 and CO_2 adsorption performance with that of Zn-TCPP-dmtrz (Fig. S9–S17). Among these materials, Al-TCPP shows the highest C_2H_2 uptake (3.89 mmol g^{-1}), but it is still lower than that of Zn-TCPP-dmtrz, while most of the other PMOFs, such as Y-TCPP, demonstrate much lower capacities due to the larger pore size weakening the interactions with C_2H_2. Interestingly, Al-TCPP and In-TCPP also exhibit relatively strong CO_2 adsorption capacities, further distinguishing Zn-TCPP-dmtrz for its superior C_2H_2/CO_2 adsorption capacity difference, highlighting its significant potential for C_2H_2/CO_2 separation.

The stability and regeneration potential of Zn-TCPP-dmtrz are evaluated through 10 adsorption–desorption cycles for both C_2H_2 and CO_2 (Fig. 2c and S18). The results indicate that the adsorption capacities are well-maintained, confirming excellent cycling stability. To further assess its separation capability, we employ the Ideal Adsorbed Solution Theory (IAST) to calculate the selectivity for C_2H_2/CO_2 (50/50). The dual-site Langmuir (DSL) model fits the adsorption isotherms with high precision (Fig. S11–S17, S19 and Table S2), and the IAST selectivity for C_2H_2/CO_2 at 298 K and 1 bar is 2.63 for Zn-TCPP-dmtrz, outperforming other TCPP-based PMOFs such as In-TCPP (2.39), Y-TCPP (1.77), and Al-TCPP (1.07) (Fig. S20). Furthermore, the maximum recoverable C_2H_2 from a C_2H_2/CO_2 mixture, represented by the separation potential (ΔQ), is calculated to be 1.62 mmol g^{-1} for Zn-TCPP-dmtrz, which is significantly higher than other PMOFs, including In-TCPP (1.10 mmol g^{-1}) (Fig. 2d). This highlights the exceptional potential of Zn-TCPP-dmtrz for efficient C_2H_2 selectivity and purification. Additionally, the adsorption heat (Q_{st}), indicative of the binding affinity between the framework and the guest molecules, is determined using adsorption isotherms at different temperatures and fitted with the Virial equation (Fig. S11–S17, S21, and Table S3). The Q_{st} for C_2H_2 is 28.5 kJ mol^{-1} at low loading, demonstrating that Zn-TCPP-dmtrz allows for energy-efficient regeneration (<30 kJ mol^{-1}), whereas the Q_{st} for CO_2 is 25.0 kJ mol^{-1}. The noticeable difference in Q_{st} supports the preferential adsorption of C_2H_2, providing moderate C_2H_2/CO_2 selectivity. Despite other PMOFs having similarly low binding energies for C_2H_2, their low adsorption capacities limit their performance in C_2H_2/CO_2 separation. In contrast, Zn-TCPP-dmtrz, as a representative of a fit-topology PMOF, combines high C_2H_2 adsorption capacity and excellent regeneration potential, making it a promising candidate for C_2H_2 purification with lower energy consumption compared to other PMOFs and conventional adsorbents (Fig. 2f).

To evaluate the practical C_2H_2/CO_2 separation performance of Zn-TCPP-dmtrz, dynamic breakthrough measurements are carried out at 298 K on a fixed-bed column packed with the activated PMOF and fed with a 50 : 50 C_2H_2/CO_2 mixture at 2 mL min^{-1} (Fig. 3a). CO_2 elutes first at 12.3 min g^{-1}, affording 9.08 $cm^3\ g^{-1}$ of 99.95% pure CO_2, whereas C_2H_2 remains on the column until 23.5 min g^{-1}, yielding a dynamic uptake of 41.22 $cm^3\ g^{-1}$ (61.1% of the 298 K isotherm capacity). In contrast, Y-TCPP demonstrates weak interactions with C_2H_2, resulting in a shorter breakthrough time for C_2H_2 (9.1 min g^{-1}), and although Al-TCPP delays C_2H_2 breakthrough to 16.4 min g^{-1}, its CO_2 elution at 19.8 min g^{-1} does not precede C_2H_2, precluding direct recovery of high-purity CO_2. Since C_2H_2 is recovered during desorption, the regeneration step is assessed by purging the saturated column with He (10 mL min^{-1}) at 333 K (Fig. 3b, S22 and S23). Zn-TCPP-dmtrz releases CO_2 completely within 4 min g^{-1}, enabling collection of C_2H_2 at >99.5% purity with a yield of 29.80 $cm^3\ g^{-1}$ (72.3% of the dynamic uptake), whereas Y-TCPP desorbs both gases rapidly—resulting in only 5.00 cm^3

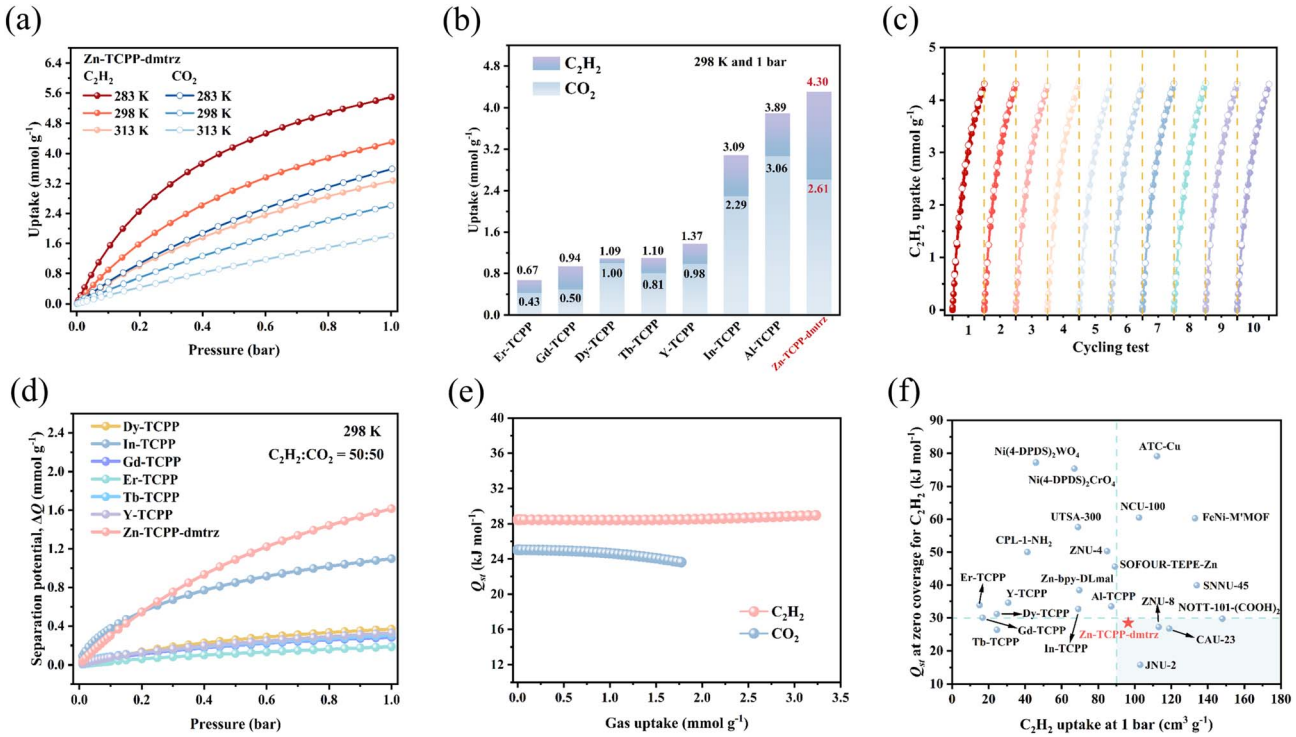

Fig. 2 (a) C_2H_2 and CO_2 adsorption isotherms of Zn-TCPP-dmtrz at 283–313 K; (b) comparison of C_2H_2 and CO_2 uptake at 298 K and 1 bar for Zn-TCPP-dmtrz and other TCPP-based PMOFs; (c) C_2H_2 adsorption isotherms of Zn-TCPP-dmtrz for 10-cycle tests at 298 K; (d) separation potential (ΔQ) curves and comparison of Zn-TCPP-dmtrz with other TCPP-based PMOFs for a 50 : 50 C_2H_2/CO_2 mixture at 298 K; (e) Q_{st} of C_2H_2 and CO_2 for Zn-TCPP-dmtrz; (f) comparison plot for Q_{st} of C_2H_2 and C_2H_2 uptake at 1 bar and 298 K.

g^{-1} C_2H_2—and Al-TCPP shows no selective C_2H_2 recovery (Fig. 3c). To probe operational feasibility, breakthrough tests under varied flow rates (3 and 5 mL min^{-1}; Fig. 3d) and temperatures (283 and 313 K; Fig. S24) maintain one-step high-purity CO_2 elution. Finally, Zn-TCPP-dmtrz retains its separation performance over five consecutive cycles without detectable change (Fig. 3e), and exhibits outstanding moisture resilience: after six months of air exposure, 48 h at 90% RH, or 24 h water immersion, PXRD patterns and 77 K N_2 isotherms show unchanged crystallinity and BET surface area (Fig. S25), and humid-condition breakthrough (Fig. 3f) yields identical elution profiles—attributable to the hydrophobic methylated triazole groups—underscoring its recyclability and stability under realistic conditions.

To gain deeper insights into the underlying mechanism of C_2H_2/CO_2 separation in Zn-TCPP-dmtrz, grand canonical Monte Carlo (GCMC) simulations and dispersion-corrected density functional theory (DFT-D) calculations are employed to probe the binding sites and interaction strengths of both gases within the framework. GCMC results reveal distinct density distributions for C_2H_2 and CO_2 within the confined pore architecture (Fig. 4a and d). Both gases localize near the porphyrin walls, aromatic rings, and alkyl-functionalized channels, but C_2H_2 exhibits significantly higher adsorption density, consistent with experimental uptake trends. Two primary adsorption sites for C_2H_2 are identified: Site I is situated near symmetrically arranged SBUs formed by TCPP porphyrin rings and dmtrz ligands, where C_2H_2 engages in multiple interactions, including hydrogen bonding between the H atoms of C_2H_2 and both the carboxylate O atoms of TCPP and the methyl H atoms of dmtrz (H···O and H···H distances ~4.0 Å) (Fig. 4b). Simultaneously, the C atoms of C_2H_2 form electrostatic interactions ($C^{\delta-}\cdots H^{\delta+}$) with aromatic H atoms (3.79–4.07 Å). Site II, located near the bilayered porphyrin region adjacent to the 10-connected Zn_5 clusters, allows C_2H_2 to form multiple $C^{\delta-}\cdots H^{\delta+}$ interactions with pyrrole moieties (3.21–3.98 Å) and engage in H···π interactions with the benzene rings (3.68 Å), as shown in Fig. 4c. In comparison, CO_2 occupies analogous regions (Fig. 4e and f) but interacts *via* weaker and fewer non-directional van der Waals forces. At Site I, CO_2 forms contacts (3.42–4.08 Å) between its O atoms and aromatic/pyrrolic H atoms, while at Site II, interactions are limited to distances of 3.57–3.99 Å. DFT-D calculations corroborate these observations: the binding energies for C_2H_2 at Sites I and II are 30.5 and 28.0 kJ mol^{-1}, respectively, significantly exceeding those for CO_2 (26.6 and 26.2 kJ mol^{-1}). These findings underscore the critical role of the densely packed π-conjugated porphyrin arrays and alkyl moieties within the ultramicroporous channels in Zn-TCPP-dmtrz, which enable enhanced C_2H_2-framework recognition through the synergistic interplay of hydrogen bonding, electrostatic complementarity, and confinement-enhanced van der Waals interactions, thereby boosting its separation performance. The results highlight the topology-guided structural design principles for developing PMOF-based materials for challenging gas separations.

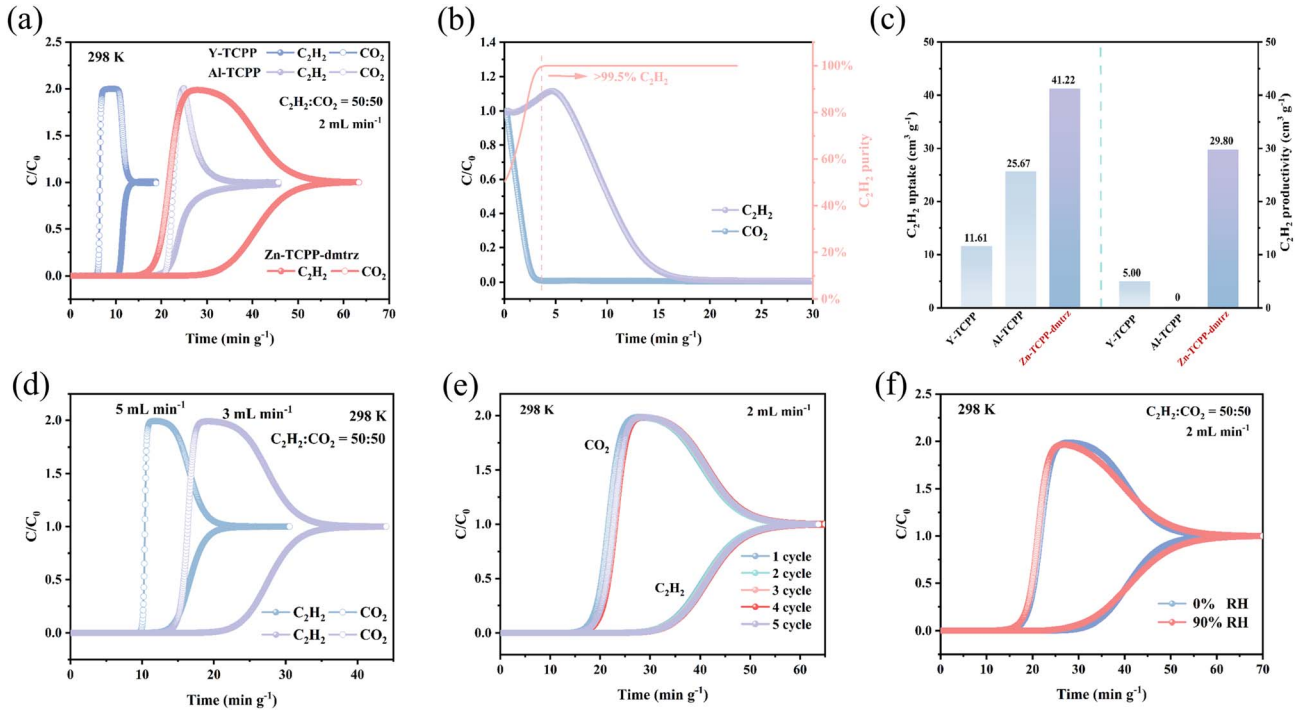

Fig. 3 Dynamic breakthrough and regeneration performance of Zn-TCPP-dmtrz and comparison with other PMOFs for C_2H_2/CO_2 (50 : 50, *v*/*v*) at 298 K: (a) breakthrough curves of Zn-TCPP-dmtrz, Al-TCPP and Y-TCPP at 2 mL min^{-1}; (b) desorption profiles of C_2H_2 and CO_2 from Zn-TCPP-dmtrz during He purge (10 mL min^{-1}) at 333 K; (c) comparison of C_2H_2 dynamic uptake and productivity among the three PMOFs; (d) breakthrough curves of Zn-TCPP-dmtrz at flow rates of 3 and 5 mL min^{-1}; (e) five consecutive breakthrough cycles for the 50 : 50 C_2H_2/CO_2 mixture; and (f) breakthrough behavior of Zn-TCPP-dmtrz under dry and humid (~90% RH) conditions.

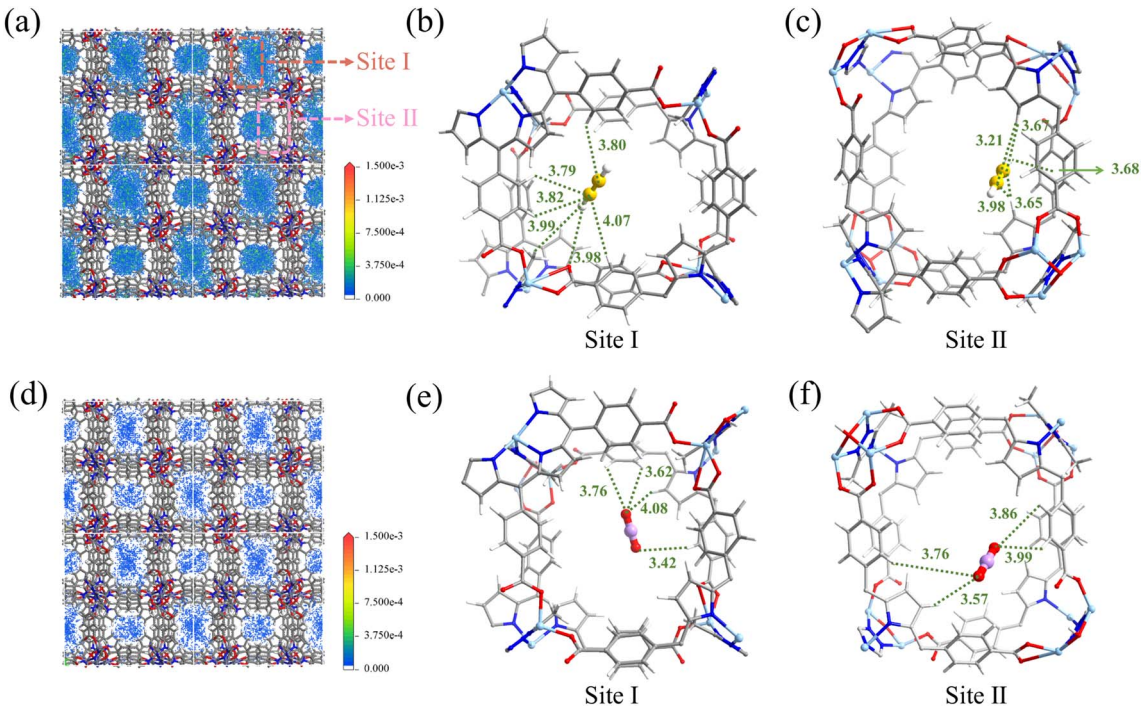

Fig. 4 Simulated adsorption density maps of (a) C_2H_2 and (d) CO_2 in Zn-TCPP-dmtrz at 298 K and 1 bar; binding configurations of C_2H_2 at (b) Site I and (c) Site II; and binding configurations of CO_2 at (e) Site I and (f) Site II. Color code: Zn-light blue, O-red, C (framework)-gray, N-blue, H-white, C (in C_2H_2)-yellow, C (in CO_2)-pink.

3. Conclusions

In summary, this study presents a strategic advancement in PMOF design by integrating Zn^{2+} coordination and dual-ligand assembly to construct an ultramicroporous architecture (6.3 × 6.8 Å) with tailored pore confinement for efficient C_2H_2/CO_2 separation. Distinct from conventional PMOFs (*e.g.*, Al- and Y-TCPP) with enlarged apertures, the Zn-TCPP-dmtrz framework adopts a novel ***fit*** topology—enabled by porphyrin chelation and triazole-mediated SBU densification—which achieves pore channels optimized for C_2H_2 accommodation. This structural design enhances host–guest interactions while maintaining framework stability, resulting in superior C_2H_2 uptake (4.30 mmol g^{-1}) and separation potential ($\Delta Q = 1.62$ mmol g^{-1}) at 298 K and 1 bar, outperforming existing PMOFs in both selectivity (2.63) and regenerability (Q_{st} = 28.5 kJ mol^{-1}). Computational analyses reveal that staggered porphyrin planes and methyl-functionalized channels synergistically amplify C_2H_2 recognition through van der Waals and electrostatic interactions—mechanisms unattainable in PMOFs with less confined geometries. Remarkable moisture resistance and cycling stability further validate its practical feasibility. By demonstrating the effectiveness of topology-driven pore engineering in PMOFs, this work expands the scope of precision adsorbent design for gas mixtures with near–identical properties, offering a blueprint for future studies to extend this strategy to other industrially relevant separations.

Author contributions

Zhenliang Zhu performed the methodology, data curation, and writing – original draft; Jianfei Xiao contributed to methodology and formal analysis; Min Zhang was involved in formal analysis; Yaoqi Huang contributed to methodology and writing – review & editing; Shaojun Yuan supervised the project, acquired funding, and contributed to project administration, resources, and writing – review & editing.

Conflicts of interest

There are no conflicts to declare.

Data availability

The data supporting this article have been included as part of the supplementary information (SI). Supplementary Information is available. See DOI: **https://doi.org/10.1039/d5sc07319g**.

Acknowledgements

The authors would like to acknowledge the financial support provided by the National Natural Science Foundation of China (22578284) and Beijing Welltrailing Science and Technology Co., Ltd (contact no. 2025510005000242) to provide financial support for this study. They also express their gratitude to Dr Ji Li and Mr Pan Wu from the Engineering Teaching Center, School of Chemical Engineering, Sichuan University, for their support in conducting the measurements using the BSD-MAB Analyzer. Furthermore, the authors would like to thank Dr Yingming Zhu from the Institute of New Energy and Low Carbon Technology, Sichuan University, for assistance with the XRD characterization. Additionally, the authors extend their gratitude to Mr Sheng Liu from Scientific Compass (**https://www.shiyanjia.com/**) for providing invaluable assistance with the single crystal structure determination.

References

1 H. W. H. Lai, F. M. Benedetti, J. M. Ahn, A. M. Robinson, Y. Wang, I. Pinnau, Z. P. Smith and Y. Xia, Hydrocarbon ladder polymers with ultrahigh permselectivity for membrane gas separations, *Science*, 2022, **375**, 1390–1392.
2 K.-J. Chen, D. G. Madden, S. Mukherjee, T. Pham, K. A. Forrest, A. Kumar, B. Space, J. Kong, Q.-Y. Zhang and M. J. Zaworotko, Synergistic sorbent separation for one-step ethylene purification from a four-component mixture, *Science*, 2019, **366**, 241–246.
3 X. Jiang, Y. Wang, H. Wang, L. Cheng, J.-W. Cao, J.-B. Wang, R. Yang, D.-H. Zhang, R.-Y. Zhang, X.-B. Yang, S.-H. Wang, Q.-Y. Zhang and K.-J. Chen, Integration of ordered porous materials for targeted three-component gas separation, *Nat. Commun.*, 2025, **16**, 694.
4 S. Capelo-Avilés, M. de Fez-Febré, S. R. G. Balestra, J. Cabezas-Giménez, R. Tomazini de Oliveira, I. I. Gallo Stampino, A. Vidal-Ferran, J. González-Cobos, V. Lillo, O. Fabelo, E. C. Escudero-Adán, L. R. Falvello, J. B. Parra, P. Rumori, G. Turnes Palomino, C. Palomino Cabello, S. Giancola, S. Calero and J. R. Galán-Mascarós, Selective adsorption of CO_2 in TAMOF-1 for the separation of CO_2/CH_4 gas mixtures, *Nat. Commun.*, 2025, **16**, 3243.
5 X. Zhang, M. Li, Y.-l. Zhao, X.-Y. Li, Y. Fang, L.-H. Xie and J.-R. Li, Simultaneous Capture of N_2O and CO_2 from a N_2O/N_2/CO_2/O_2 Mixture with a Ni(II)-Pyrazolecarboxylate Framework, *J. Am. Chem. Soc.*, 2025, **147**(20), 17042–17048.
6 M. Yi, S. Wang, S. Li, S. Zhang, Y. Liu, L. Zhang, Z. You, X. Liu, L. Li, J. Wang, H. Wang, Q. Zhao, B. Li and X.-H. Bu, Superhydrophobic Molecular Selector for Efficient Separation of Ethane over Ethylene under Dry and Humid Conditions, *J. Am. Chem. Soc.*, 2025, **147**, 13592–13600.
7 T. Li, P. Cui and D. Sun, Uncoordinated Hexafluorosilicates in a Microporous Metal–Organic Framework Enabled C_2H_2/CO_2 Separation, *Inorg. Chem.*, 2022, **61**, 4251–4256.
8 S.-Q. Yang, R. Krishna, H. Chen, L. Li, L. Zhou, Y.-F. An, F.-Y. Zhang, Q. Zhang, Y.-H. Zhang, W. Li and T.-L. Hu, Immobilization of the polar group into an ultramicroporous metal–organic framework enabling benchmark inverse selective CO_2/C_2H_2 separation with record C_2H_2 production, *J. Am. Chem. Soc.*, 2023, **145**, 13901–13911.
9 S.-Q. Yang, B. Xing, L.-L. Wang, L. Zhou, F.-Y. Zhang, Y.-L. Li and T.-L. Hu, Boosting Acetylene Packing Density within an Isoreticular Metal–Organic Framework for Efficient C_2H_2/CO_2 Separation, *Chem. Biol. Eng.*, 2024, **1**, 245–251.

10 W. Chen, P. Cai, H. C. Zhou and S. T. Madrahimov, Bridging Homogeneous and Heterogeneous Catalysis: Phosphine-Functionalized Metal-Organic Frameworks, *Angew. Chem., Int. Ed.*, 2024, **63**, e202315075.

11 R. R. Liang, Z. Liu, Z. Han, Y. Yang, J. Rushlow and H. C. Zhou, Anchoring Catalytic Metal Nodes within a Single-Crystalline Pyrazolate Metal-Organic Framework for Efficient Heterogeneous Catalysis, *Angew. Chem., Int. Ed.*, 2025, **64**, e202414271.

12 J. He, G. Wen, Q. Peng and X. Hou, The design, synthesis and application of metal–organic framework-based fluorescence sensors, *Chem. Commun.*, 2024, **60**, 11237–11252.

13 S.-M. Wang, L. Xu, L.-P. Zhang, Y.-T. Li, T. Wang and Q.-Y. Yang, Rational Design of a π-Electron Rich Co-MOF Enabling Benchmark C_2H_6/CH_4 Selectivity in Natural Gas Purification, *Adv. Funct. Mater.*, 2025, 2504251.

14 H. Kim, Y. Seo, J. Park, E. Lee and H. Oh, A Gate-Opening Control Strategy via Nitrate–Chloride Anion Exchange for Enhanced Hydrogen Isotope Separation in Metal–Organic Frameworks, *Angew. Chem., Int. Ed.*, 2025, **64**, e202421756.

15 G. Lee, D. Choi and M. Oh, Activating the Gate-Opening of a Metal–Organic Framework and Maximizing Its Adsorption Capacity, *J. Am. Chem. Soc.*, 2025, **147**, 12811–12820.

16 Y.-Z. Hao, K. Shao, X. Zhang, Y.-H. Yu, D. Liu, H.-M. Wen, Y. Cui, B. Li, B. Chen and G. Qian, Pore Space Partition Enabled by Lithium(I) Chelation of a Metal–Organic Framework for Benchmark C_2H_2/CO_2 Separation, *J. Am. Chem. Soc.*, 2025, **147**, 11257–11266.

17 Z. Zhu, J. Xiao, M. Zhang, Y. Wang, K. Xin Yao and S. Yuan, Nonpolar microporous Metal-Organic framework decorated with multiple functional sites for efficient Ethane/Ethylene separation, *Sep. Purif. Technol.*, 2025, **354**, 128696.

18 J. Xiao, Z. Zhu, M. Zhang, Y. Huang, T. C. Zhang and S. Yuan, Efficient One-Step Purification of Methanol-to-Olefin Products Using a Porphyrinyl MOF to Achieve Record C_2H_4 and C_3H_6 Productivity, *ACS Appl. Mater. Interfaces*, 2025, **17**, 21630–21642.

19 M. Jung, J. Park, R. Muhammad, T. Park, S.-Y. Jung, J. Yi, C. Jung, J. Ollivier, A. J. Ramirez-Cuesta, J. T. Park, J. Kim, M. Russina and H. Oh, Lattice-driven gating in a Cu-based zeolitic imidazolate framework for efficient high-temperature hydrogen isotope separation, *Nat. Commun.*, 2025, **16**, 2032.

20 B. Pramanik, R. Sahoo, R. Krishna and M. C. Das, A Chemically Robust Microporous Zn-MOF for C_2H_2 Separation from CO_2 and Industrially Relevant Four Component Gas Mixtures, *Small*, 2025, **21**, 2411456.

21 S. S. Y. Chui, S. M. F. Lo, J. P. H. Charmant, A. G. Orpen and I. D. Williams, A chemically functionalizable nanoporous material $[Cu_3(TMA)_2\ (H_2O)_3]_{(n)}$, *Science*, 1999, **283**, 1148–1150.

22 J.-S. Zou, Z.-P. Wang, Y. H. Andaloussi, J. Xue, W. Zhang, B. E. G. Lucier, Z. Zhang, Y. Jia, X.-C. Wu, J. Li, Y. Huang, M. J. Zaworotko, G. Chen, S. Chen and Y.-L. Peng, Benchmarking selective capture of trace CO_2 from C_2H_2 using an amine-functionalized adsorbent, *Nat. Commun.*, 2025, **16**, 2598.

23 Y. Zhang, Y. Han, B. Luan, L. Wang, W. Yang, Y. Jiang, T. Ben, Y. He and B. Chen, Metal–Organic Framework with Space-Partition Pores by Fluorinated Anions for Benchmark C_2H_2/CO_2 Separation, *J. Am. Chem. Soc.*, 2024, **146**, 17220–17229.

24 Y.-L. Zhao, Q. Chen, X. Zhang and J.-R. Li, Enabling C_2H_2/CO_2 Separation Under Humid Conditions with a Methylated Copper MOF, *Adv. Sci.*, 2024, **11**, 2310025.

25 L. Zhang, T. Xiao, X. Zeng, J. You, Z. He, C.-X. Chen, Q. Wang, A. Nafady, A. M. Al-Enizi and S. Ma, Isoreticular Contraction of Cage-like Metal–Organic Frameworks with Optimized Pore Space for Enhanced C_2H_2/CO_2 and C_2H_2/C_2H_4 Separations, *J. Am. Chem. Soc.*, 2024, **146**, 7341–7351.

26 D. Song, S. Zou, Z. Ji, Y. Li, H. Li, Y. Zhou, C. Chen, Q. Chen and M. Wu, One-Step Ethylene Purification from Ternary Mixture through Adaptive Recognition Sites, *Angew. Chem., Int. Ed.*, 2025, **64**, e202423496.

27 F. Yuan, Y. Li, Z. Yuan, L. Li, C. Chen, L. He, H. Lin, X. Fan, B. Chen, S. Xiang and Z. Zhang, A Grafting Hydrogen-bonded Organic Framework for Benchmark Selectivity of C_2H_2/CO_2 Separation under Ambient Conditions, *Angew. Chem., Int. Ed.*, 2025, **64**, e202414215.

28 Y.-Z. Hao, H.-M. Wen, Y.-H. Yu, X. Zhang, Y. Cui, B. Chen, B. Li and G. Qian, Anchoring Highly Unsaturated Nickel(II) Sites into a Metal–Organic Framework for Simultaneous High C_2H_2 Adsorption and Separation, *Angew. Chem., Int. Ed.*, 2025, e202506055.

29 P. Zhang, Y. Zhong, Y. Zhang, Z. Zhu, Y. Liu, Y. Su, J. Chen, S. Chen, Z. Zeng and H. Xing, Synergistic binding sites in a hybrid ultramicroporous material for one-step ethylene purification from ternary C2 hydrocarbon mixtures, *Sci. Adv.*, 2022, **8**, eabn9231.

30 Y. Wang, C. Hao, W. Fan, M. Fu, X. Wang, Z. Wang, L. Zhu, Y. Li, X. Lu, F. Dai, Z. Kang, R. Wang, W. Guo, S. Hu and D. Sun, One-step Ethylene Purification from an Acetylene/Ethylene/Ethane Ternary Mixture by Cyclopentadiene Cobalt-Functionalized Metal–Organic Frameworks, *Angew. Chem., Int. Ed.*, 2021, **60**, 11350–11358.

31 M. Sun, H. Liu, X. Wang, X. Yang, F. Gao, D. Xie, W. Fan, Y. Han, B. Xu and D. Sun, Metal-ion-tuned metal-organic frameworks for C_2H_2/CO_2 separation, *Chin. J. Struct. Chem.*, 2023, **42**, 100146.

32 L. Xu, M.-K. Zhai, F. Wang, L. Sun and H.-B. Du, A series of robust metal–porphyrinic frameworks based on rare earth clusters and their application in N–H carbene insertion, *Dalton Trans.*, 2016, **45**, 17108–17112.

33 X. He, S. Gao, R. Peng, D. Zhu and F. Yu, A novel topological indium–organic framework for reversible ammonia uptake under mild conditions and catalysis, *J. Mater. Chem. A*, 2024, **12**, 14501–14507.

34 M. V. Nguyen, H. C. Dong, V. T. N. Truong, H. N. Nguyen, L. C. Luu, N. N. Dang and T. A. T. Nguyen, A new porphyrinic vanadium-based MOF constructed from infinite $V(OH)O_4$ chains: syntheses, characterization and

photoabsorption properties, *New J. Chem.*, 2022, **46**, 632–641.

35 R. L. Mander, A. Schmidt, M. Ruf and M. D. Korzyński, Design and synthesis of pillared metal–organic frameworks featuring olefinic fragments, *Dalton Trans.*, 2024, **53**, 18873–18879.

36 E.-Y. Choi, C. A. Wray, C. Hu and W. Choe, Highly tunable metal–organic frameworks with open metal centers, *CrystEngComm*, 2009, **11**, 553–555.

37 Z. Zhu, J. Xiao, M. Zhang, Y. Huang and S. Yuan, Two isostructural pillar-layered metal-organic frameworks with hydrophobic properties for efficient C_2H_6/C_2H_4 separation under humid conditions, *Sep. Purif. Technol.*, 2025, **361**, 131343.

38 Z.-H. Guo, X.-Q. Wu, Y.-P. Wu, D.-S. Li, G.-P. Yang and Y.-Y. Wang, A Scalable Pore-space-partitioned Metal-organic Framework Powered by Polycatenation Strategy for Efficient Acetylene Purification, *Angew. Chem., Int. Ed.*, 2025, **64**, e202421992.

39 J.-W. Cao, T. Zhang, Y.-Q. Liu, Y. Wang, F.-P. Pan, J. Chen and K.-J. Chen, Precise C_2H_2 Adsorption Affinity Modulation by Nitrogen Functionalization in Isostructural Coordination Networks, *Small*, 2025, **21**, 2501924.

40 A. Fateeva, J. Clarisse, G. Pilet, J.-M. Grenèche, F. Nouar, B. K. Abeykoon, F. Guegan, C. Goutaudier, D. Luneau, J. E. Warren, M. J. Rosseinsky and T. Devic, Iron and Porphyrin Metal–Organic Frameworks: Insight into Structural Diversity, Stability, and Porosity, *Cryst. Growth Des.*, 2015, **15**, 1819–1826.

41 X.-N. Wang, J.-L. Li, Y.-M. Zhao, J. Pang, B. Li, T.-L. Zhang and H.-C. Zhou, Structural tuning of zinc–porphyrin frameworks via auxiliary nitrogen-containing ligands towards selective adsorption of cationic dyes, *Chem. Commun.*, 2019, **55**, 6527–6530.

42 Q. Ding, Z. Zhang, Y. Liu, K. Chai, R. Krishna and S. Zhang, One-Step Ethylene Purification from Ternary Mixtures in a Metal–Organic Framework with Customized Pore Chemistry and Shape, *Angew. Chem., Int. Ed.*, 2022, **61**, e202208134.

43 D. Jia, Z. Shen, W. Zhou, Y. Li, J. He, L. Jiang, Y. Wei and X. He, Ultrahigh N-doped carbon with hierarchical porous structure derived from metal-organic framework for high-performance zinc ion hybrid capacitors, *Chem. Eng. J.*, 2024, **485**, 149820.

44 J. Liu, H. Xiong, H. Shuai, X. Liu, Y. Peng, L. Wang, P. Wang, Z. Zhao, Z. Deng, Z. Zhou, J. Chen, S. Chen, Z. Zeng, S. Deng and J. Wang, Molecular sieving of iso-butene from C4 olefins with simultaneous high 1,3-butadiene and n-butene uptakes, *Nat. Commun.*, 2024, **15**, 2222.

45 X. Liu, P. Zhang, H. Xiong, Y. Zhang, K. Wu, J. Liu, R. Krishna, J. Chen, S. Chen, Z. Zeng, S. Deng and J. Wang, Engineering Pore Environments of Sulfate-Pillared Metal-Organic Framework for Efficient C_2H_2/CO_2 Separation with Record Selectivity, *Adv. Mater.*, 2023, **35**, 2210415.

46 J. Pei, K. Shao, J. X. Wang, H. M. Wen, Y. Yang, Y. Cui, R. Krishna, B. Li and G. Qian, A Chemically Stable Hofmann-Type Metal–Organic Framework with Sandwich-Like Binding Sites for Benchmark Acetylene Capture, *Adv. Mater.*, 2020, **32**, 1908275.

47 H. Zeng, M. Xie, Y. L. Huang, Y. Zhao, X. J. Xie, J. P. Bai, M. Y. Wan, R. Krishna, W. Lu and D. Li, Induced fit of C_2H_2 in a flexible MOF through cooperative action of open metal sites, *Angew. Chem., Int. Ed.*, 2019, **58**, 8515–8519.

48 S. Shang, Z. Zhou, H. Wang, Y. Wang, X. Liu, Z. Zhu, Y. Zeng, C. Liu, H. Xiong, H. Liu, F. Zhao, J. Chen, S. Chen, Z. Zhou and J. Wang, A Rigid, Stable, and Scalable Aliphatic MOF Adsorbent for Efficient C_2H_2/CO_2 Separation with Record Acetylene Packing Density, *Angew. Chem., Int. Ed.*, 2025, e202503317.

49 Y. L. Peng, T. Pham, P. Li, T. Wang, Y. Chen, K. J. Chen, K. A. Forrest, B. Space, P. Cheng and M. J. Zaworotko, Robust ultramicroporous metal–organic frameworks with benchmark affinity for acetylene, *Angew. Chem., Int. Ed.*, 2018, **57**, 10971–10975.